JOURNAL OF THERMOPHYSICS AND HEAT TRANSFER
Vol. 25, No. 1, January–March 2011

Effect of Dimple Configuration on Heat Transfer Coefficient in a Rotating Channel

Seokbeom Kim,* Young Jin Lee,* Eun Yeong Choi,* and Jae Su Kwak†
Korea Aerospace University, Goyang-City 412-791, Republic of Korea

DOI: 10.2514/1.50255

The detailed distribution of heat transfer coefficients in a rotating dimpled rectangular channel (aspect ratio =6 and 12) was measured by the transient liquid crystal technique. The rotating speed of the channel was fixed at 500 rpm and the tested Reynolds number based on the channel hydraulic diameter was varied from 19,000 to 44,000. Four different dimple configurations were tested to investigate the effects of relative dimple depth, dimple center distance, and channel height on the heat transfer coefficient. A stationary case and two different rotating directions were tested so that the dimple fabricated surface became the trailing or leading surface. Results showed that the heat transfer coefficient on the dimpled surface was higher if the dimpled surface became a trailing surface. Also, with the same dimple diameter, higher heat transfer coefficients were observed for deeper dimple, narrower channel or densely distributed dimple cases.

Nomenclature

D	=	dimple printed diameter
D_h	=	hydraulic diameter
d	=	dimple depth
f	=	Darcy friction factor
f_0	=	Darcy friction factor for a smooth duct
H	=	channel height
h	=	heat transfer coefficient
k	=	thermal conductivity of test section
k_m	=	thermal conductivity of air
Nu	=	Nusselt number for a hydraulic diameter $=(hD_h/k_m)$
Nu_0	=	Nusselt number for a smooth duct
Pr	=	Prandtl number of air
Re	=	Reynolds number $=(VD_h/\nu)$
S	=	dimple center-to-center distance
t	=	transient time
u	=	averaged mainstream velocity
V	=	fluid velocity
W	=	channel width
X_s	=	the starting point distance of heat transfer measurement area
α	=	thermal diffusivity of test section
Δp	=	pressure drop through the test section
Δx	=	distance between pressure taps
ρ_m	=	density of air
ν	=	kinematic viscosity of air

I. Introduction

INCREASING the gas turbine inlet temperature (TIT) is one of the most effective methods for improving the thermal performance of a gas turbine and the TIT of a modern gas turbine exceeds the permissible operating temperature of a gas turbine blade's material. So, various cooling techniques have been studied to ensure the durability and life of gas turbine blades [1]. Blade cooling systems could be selected by considering the degree of heat transfer augmentation, the pressure drop through the cooling channel, and manufacturing simplicity. It is known that a dimpled surface increases heat transfer with a lower pressure drop compared with the rib turbulated cooling technique which is widely used in gas turbine blades. Also, because a surface with dimples requires generally uncomplicated fabricating procedures, a heat transfer augmenting technique using dimples has been studied for a blade cooling system in gas turbines [2].

Belen'kiy et al. [3] investigated the effect of dimple configuration on heat transfer coefficient and their results showed that a surface with spherical cavities induced a higher heat transfer coefficient than a smooth surface. Moon et al. [4] studied the effect of Reynolds numbers and channel heights H on the heat transfer of dimpled surfaces, and concluded that thermal performance and friction factors are scarcely affected by the ratio of channel height to dimple diameter H/D. Mahmood et al. [5] measured the heat transfer coefficient on a oneside dimple surface, and showed that the vortex shed from dimples augmented the Nusselt number near the downstream rim of the dimple. Also, they indicated that this phenomenon was prominent as the ratio of inlet stagnation temperature to surface temperature decreased.

Moon and Lau [6] investigated the effect of dimple shape and dimple configurations on heat transfer augmentation and reported that a cylindrical shaped dimple induced a higher thermal performance than a concave shape. Griffith et al. [7] measured the averaged heat transfer coefficient in a rotating channel with both sides dimpled and investigated the effects of channel orientation and rotation number on the heat transfer. Mahmood and Ligrani [8] carried out flow visualizations and heat transfer measurements to investigate the effects of Reynolds number, temperature ratio, and nondimensional channel height H/D on the flow and heat transfer coefficient in a dimpled channel. Flow visualization results showed periodically shedding vortex pairs from the dimples. The vortex pairs became stronger as the H/D value decreased, which led to local Nusselt number augmentation for $H/D < 1$.

Wang et al. [9] conducted computational studies on a single or multiple dimpled surface, and showed flow patterns near dimples in a low Reynolds number condition. Burgess and Nigrani [10] concentrated on the influence of the dimple depth d on the heat transfer augmentation and concluded that the heat transfer coefficient on the dimpled surface increased as the dimple depth increased, which is caused by an increase in the strengths of vortices, associated secondary flows ejected from the dimples, and an increase in the magnitudes of three-dimensional turbulence production and turbulence transport. Khalatov et al. [11] carried out flow visualizations for rows of cylindrical or spherical dimples, and showed that the flow pattern in and near a dimple was strongly affected by Reynolds number, configuration of dimple, and existence of other dimples.

Received 12 April 2010; revision received 27 September 2010; accepted for publication 14 October 2010.

*Graduate Student, School of Aerospace and Mechanical Engineering.
†Assistant Professor, School of Aerospace and Mechanical Engineering; jskwak@kau.ac.kr (Corresponding Author).

Ligrani et al. [12] studied the effect of Reynolds number, dimple depth, and turbulence intensity on the flow patterns and heat transfer coefficients on the dimpled surface. Their results showed that the Nusselt number ratio and friction factor were slightly increased as the turbulence intensity increased. Also, the Nusselt number increased as the dimple depth increased and the highest Nusselt number was observed near the dimple's downstream edge. Shin et al. [13] measured the detailed heat transfer coefficient distribution on a oneside dimpled test section and concluded that the heat transfer coefficient and the thermal performance factor were higher for lower channel height cases. Slabaugh et al. [14] performed heat transfer measurements on dimpled surfaces with various dimple configurations, and indicated that the double dimpled surface showed higher heat transfer augmentation. Elyyan and Tafti [15] carried out the computational heat transfer studies for the rotating channel with dimples and protrusions. They concluded that heat transfer performance on the trailing surface was higher for the protrusions at low rotation number ($|R_o| < 0.2$), whereas that was higher for the dimple at higher rotation number ($|R_o| > 0.2$). They also showed that the deeper dimple (protrusion) presents higher heat transfer augmentation.

Most previous experimental studies on heat transfer enhancement due to dimples have been conducted in a stationary channel and could not simulate the rotational effect. Though Griffith et al. [7] presented experimental data for a rotating dimpled channel, their results showed the averaged heat transfer coefficient for only one dimple configuration and channel height.

In this study, detailed distributions of the heat transfer coefficients in a rotating dimpled channel were measured by the transient liquid crystal technique. Three dimple configurations, two channel heights, three rotating conditions, and three Reynolds numbers were tested to investigate the effects of dimple depth, channel height, dimple center-to-center distance, rotating direction, and rotation number on the heat transfer coefficient. In the authors' knowledge, this study is the first experimental data available in the open literature for the distribution of heat transfer coefficient in a rotating dimpled channel with various dimple configurations and channel heights. The results presented in this paper could be used for the computational fluid dynamics (CFD) code validation.

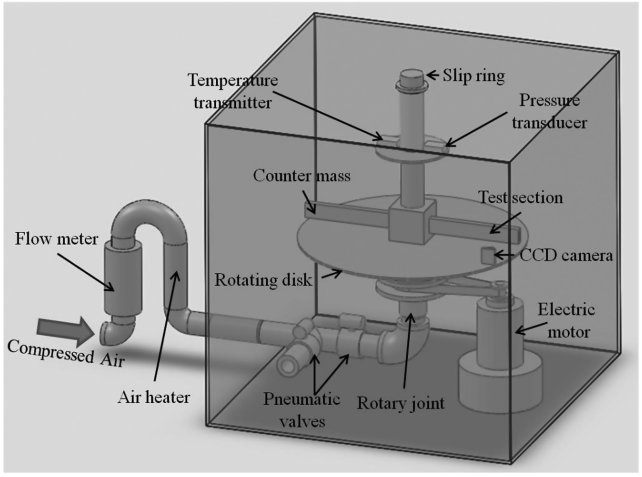

Fig. 1 Schematic of the test facility.

II. Experimental Apparatus

Figure 1 shows a schematic of the test apparatus which consists of a blower, a flow meter (PA-601, Flownics), an air heater (3 KW), two pneumatic valves, a rotary joint, a slip ring for data transmission, and a digital charge-coupled device (CCD) camera (FireWire-A BCL 1.2, Edmunds Optics) mounted on the rotating disk. Compressed air was heated by the air heater and bypassed until the air temperature reached a predetermine value. After the air temperature reached a sufficient level, the air was diverted into a rotary joint so that the heated air could be supplied to the rotating hollow shaft and test section.

Figure 2a presents the detailed view of the test section. The test section was made of 10 mm thick polycarbonate plate and dimples were fabricated on oneside of the wall. Black paint and liquid crystals

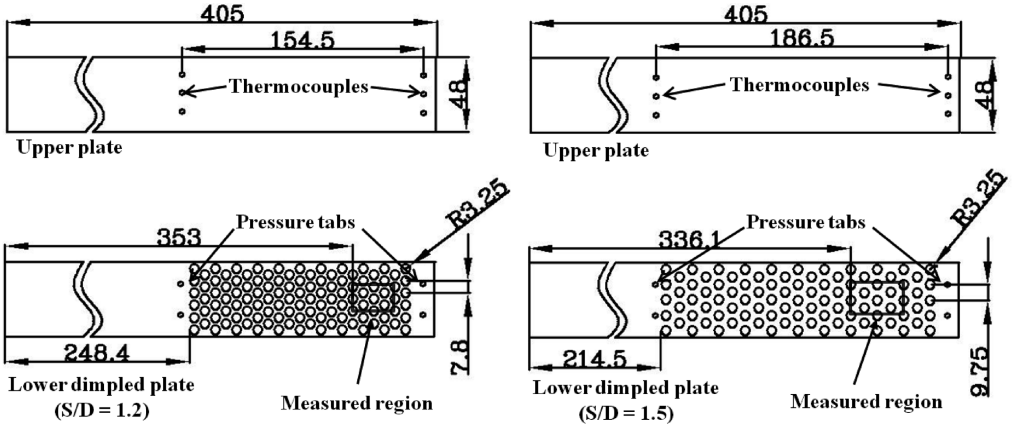

a) Detailed view of the test section

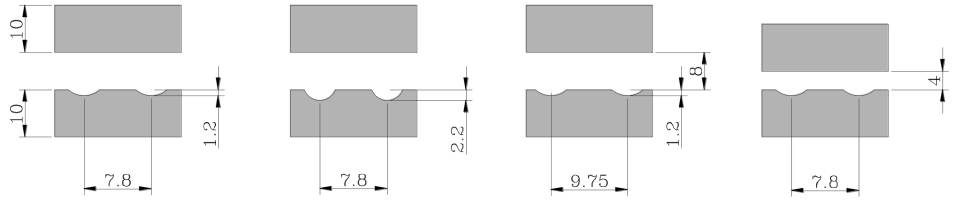

b) Configuration of dimple and channel height

Fig. 2 Configurations of the test section (all dimensions in mm).

Table 1 Specifications of the tested dimpled channel

Configuration	A	B	C	D
Dimple diameter (D)	6.5 mm	6.5 mm	6.5 mm	6.5 mm
Dimple depth (d)	1.2 mm	2.2 mm	1.2 mm	1.2 mm
Dimple center-to-center distance (S)	7.8 mm	7.8 mm	9.75 mm	7.8 mm
Channel height (H)	8 mm	8 mm	8 mm	4 mm
Channel width (W)	48 mm	48 mm	48 mm	48 mm
H/D	1.23	1.23	1.23	0.615
S/D	1.2	1.2	1.5	1.2
d/D	0.185	0.338	0.185	0.185
Hydraulic diameter (D_h)	0.013714 m	0.013714 m	0.013714 m	0.007385 m
Channel aspect ratio (W/H)	6	6	6	12

with a bandwidth of 1°C (35C1W, Hallcrest) were sprayed on the dimpled wall. During the heat transfer measurement, the liquid crystals color change was captured by a digital CCD camera which rotated with the test section. From the history of the liquid crystals color change, the transient time was calculated by a Matlab based image processing program. The detailed image process was explained by Shin et al. [13].

During the transient tests, the mainstream temperature change was measured by six T-type thermocouples installed up and downstream of the test section as shown in Fig. 2a. On the dimpled wall, pressure taps were installed to measure pressure loss in the dimpled channel. The digital CCD camera signal, temperature, and pressure data were transferred to a PC through a 24-channel slip ring. Three dimple configurations and two channel heights were tested as shown in Fig. 2b to investigate the effects of dimple depth, dimple center-to-center distance and channel height on the heat transfer on the dimpled surface and pressure drop through the channel. Detailed configurations of the test sections are listed in Table 1.

To ensure a periodically fully developed heat transfer condition on the heat transfer measuring area, a total of 21 rows of dimples were fabricated and the heat transfer coefficient was measured between 16 and 20 rows (for configurations A, B, and D) or between 15 and 19 rows of dimples (for configuration C). Channel hydraulic diameter, D_h for configurations A, B, and C is 13.714 mm and D_h for configuration D is 7.385 mm, respectively. The heat transfer measurement area begins at 353 mm ($x/D_h = 25.74$) for configurations A and B, 336.1 mm ($x/D_h = 24.51$) for configuration C, and 353 mm ($x/D_h = 47.8$) for configuration D, respectively. The location of heat transfer measurement region is shown in Fig. 2.

For all tested cases, the rotating speed of the dimpled channel was fixed at 500 rpm and three Reynolds numbers based on a channel hydraulic diameter of 19,000, 31,000, and 44,000 were tested. The corresponding rotation number R_o, defined by Eq. (1), ranged between 0.0149 and 0.0345 (for configuration A, B, C), between 0.0043 and 0.0099 (for configuration D)

$$R_o = \frac{\omega D_h}{V} \tag{1}$$

Figure 3 illustrates three different rotating conditions of the test section. Depending on the rotation direction, the dimpled surface became a trailing surface (TS case) or a leading surface (LS case). For comparison, stationary cases (ST case) were also tested.

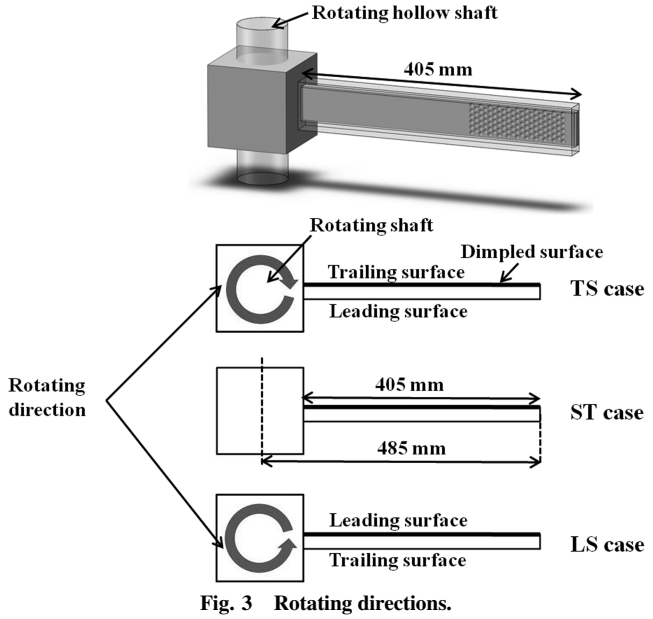

Fig. 3 Rotating directions.

III. Experimental Theory

For the heat transfer coefficient measurement by the transient liquid crystal technique, the test surface is assumed to be a semi-infinite solid wall with a convective boundary condition. If a sudden change in mainstream temperature is applied, the surface temperature can be expressed as Eq. (2)

$$\frac{T_w - T_i}{T_m - T_i} = 1 - \exp\left(\frac{h^2 \alpha t}{k^2}\right) \mathrm{erfc}\left(\frac{h\sqrt{\alpha t}}{k}\right) \tag{2}$$

For the current test set up, the mainstream temperature varies with time. The varying mainstream temperature can be viewed as a series of step changes and the surface temperature can be expressed as Eq. (3)

$$T_w - T_i = (T_{m,0} - T_i) \times F\left(\frac{h\sqrt{\alpha t}}{k}\right) + \sum_{i=1}^{n}\left[F\left(\frac{h\sqrt{\alpha(t-\tau_i)}}{k}\right)\Delta T_{m,i}\right]$$
$$\text{where, } F(x) = 1 - \exp(x^2)\mathrm{erfc}(x) \tag{3}$$

Once the time t from the initial temperature T_i to the predefined temperature T_w is determined by the image processing procedure, the heat transfer coefficient can be calculated by Eq. (3). The mainstream temperature T_m is measured by T-type thermocouples installed upstream and downstream of the test section as shown in Fig. 2a. The mainstream temperature for the heat transfer calculation at each pixel was evaluated based on the distance between the thermocouples and each pixel.

During the transient tests, the heated mainstream air was supplied to the channel and the liquid crystals coated surface was heated. Because the temperatures of mainstream air and surface continuously changed, the inlet coolant-to-wall density ratio or buoyancy parameter could not be defined.

Nusselt number is defined by Eq. (4) and the Nusselt number for a fully developed turbulent flow in a smooth duct, Nu_0, can be calculated by Eq. (5) [16]

$$Nu = \frac{hD_h}{k_m} \tag{4}$$

$$Nu_0 = \frac{(f_0/8)(Re_{Dh} - 1000)Pr}{[1 + 12.7(f_0/8)^{1/2}(Pr^{2/3} - 1)]}$$
$$\text{for } 0.5 < Pr < 2000 \qquad 3000 < Re_{Dh} < 5 \times 10^6 \tag{5}$$

f_0 in Eq. (5) is friction factor for fully developed turbulent flow in a smooth duct calculated by Eq. (6) [16]

$$f_0 = [0.79(Re_{D_h}) - 1.64]^{-2} \quad \text{for } 3,000 < Re_{Dh} < 5 \times 10^6 \tag{6}$$

Pressure drop through the dimpled channel can be expressed in term of the Darcy friction factor f defined by Eq. (7). In Eq. (7), the pressure drop Δp was measured by four pressure taps shown in Fig. 2a

$$f = \frac{-(\Delta p/\Delta x)D_h}{\rho_m u^2/2} \tag{7}$$

During the transient tests, the heat transfer on the test section is assumed to be a one-dimensional heat transfer, the test duration must be limited for the opposite side of the test section to remain at the initial temperature. Wagner et al. [17] suggested a criterion for the transient test duration time as Eq. (8)

$$\frac{\alpha t_{\text{test duration}}}{\text{thickness}^2} < \frac{1}{4} \tag{8}$$

For our tested condition, $t_{\text{test duration}}$ by Eq. (8) is about 180 s and the transient test duration was kept below 90 s.

Uncertainty of the measured heat transfer coefficient and Nusselt number was estimated using procedures presented by Moffat [18]. Based on a 95% confidence level, the uncertainties of the measured heat transfer coefficient, Nusselt number, and friction factor are estimated as ±7.3%, ±8.5%, and ±6.5%, respectively.

IV. Result and Discussion

Figure 4 presents the distribution of Nusselt numbers for configuration A, the TS case for varying Reynolds numbers, and clearly shows the high and low Nusselt numbers inside and near the dimples. The overall Nusselt number increases as the Reynolds number increases. For all Reynolds number cases, the lowest Nusselt number is observed on the concavity floor facing upstream and the highest Nussselt number can be seen in the vicinity of the downstream edge of the dimples. The low Nusselt number on the dimple cavity floor is caused by the flow separation and recirculation near the upstream dimple edge, and the high Nusselt number near the downstream edge of the dimple is induced by the flow reattachment and multiple vortex pairs, which are periodically shed from each dimple as discussed by Mahmood et al. [5] and Ligrani et al. [12].

Figure 5 is the Nusselt number distribution of configuration A for the same Reynolds number of 19,000 with different rotating directions. The overall Nusselt number is highest for the TS case followed by ST and LS cases. With rotation, the mainstream flow shifted toward the trailing surface due to the Coriolis force and the heat transfer on the trailing surface increases. Because of the enhanced heat transfer on the trailing surface, the flow temperature near the trailing surface is lower than that near the leading surface, (density near the trailing surface is higher than that near the leading surface) and the lower temperature fluid particles near the trailing surface are accelerated by the centrifugal force. This is called the rotational buoyancy force. Because of the Coriolis force and the rotational buoyancy force, the Nusselt number on the dimpled surface is higher for the TS case than the LS case.

Figure 6 shows the Nusselt number distribution in a streamwise direction along the center of the channel for $Re = 19,000$. All cases show a periodically fully developed Nusselt number pattern. The highest Nusselt numbers are observed near the dimple downstream

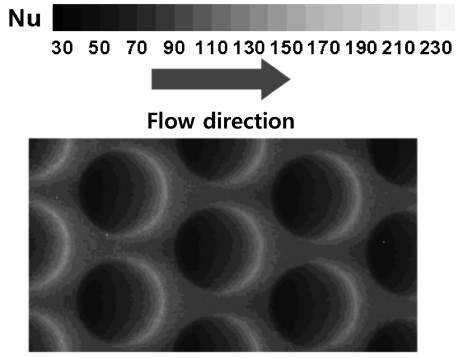

a) Re = 19,000 (Ro = 0.0345)

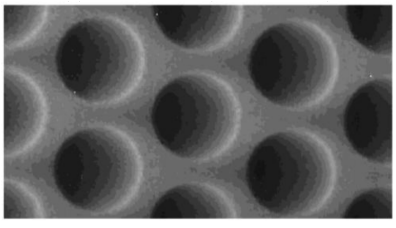

b) Re= 31,000 (Ro = 0.0211)

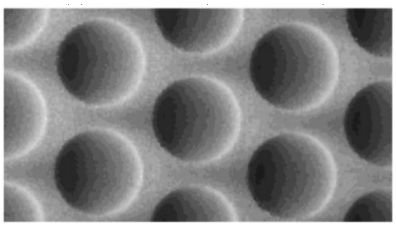

c) Re = 44,000 (Ro = 0.0149)

Fig. 4 Nusselt number distribution for configuration A, TS case.

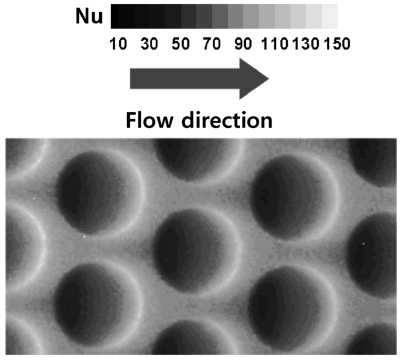

a) TS

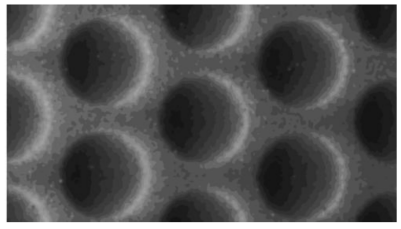

b) ST

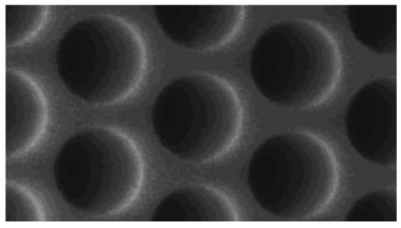

c) LS

Fig. 5 Nusselt number distribution for configuration A ($Re = 19,000$, $R_o = 0.0345$).

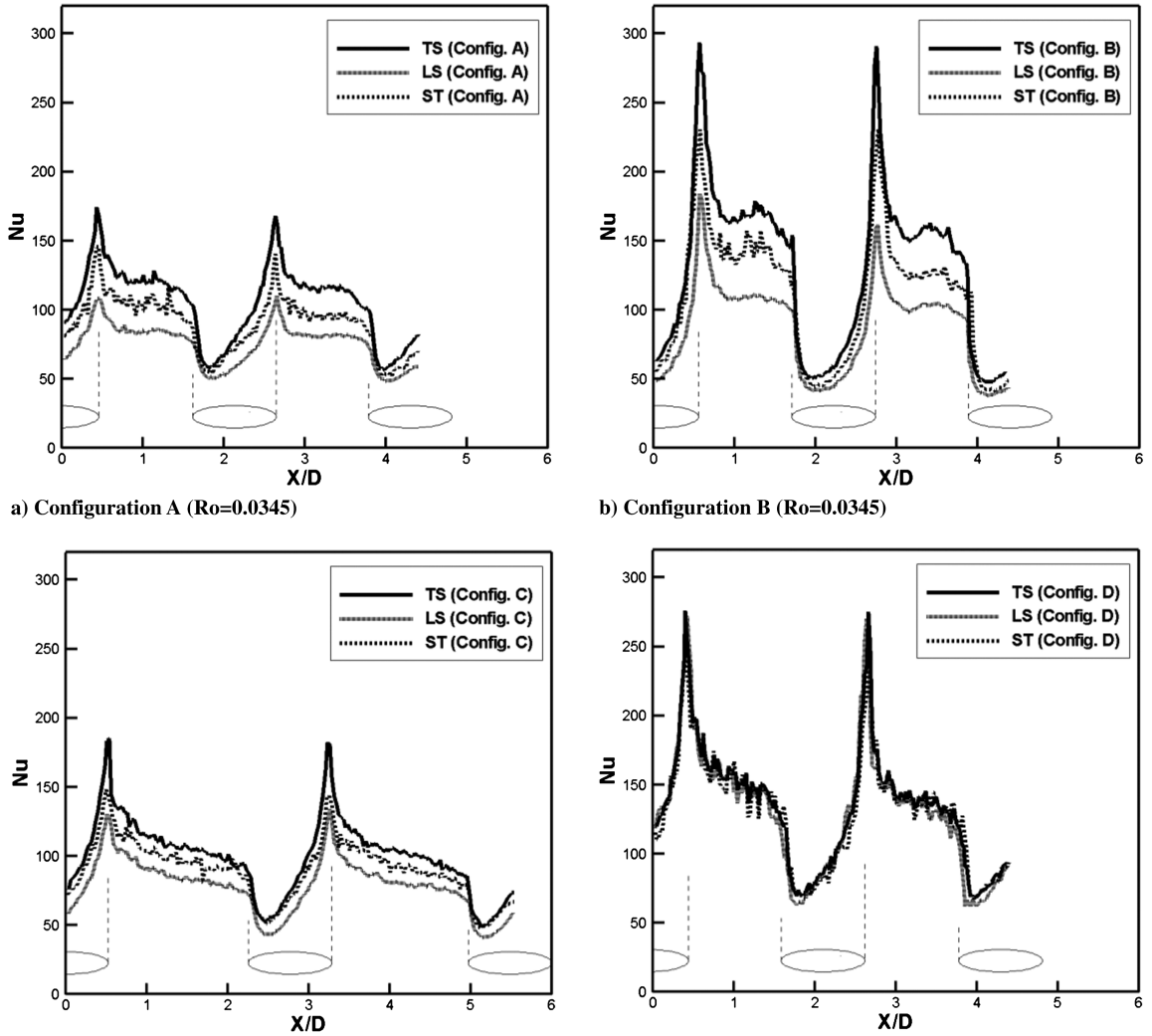

a) Configuration A (Ro=0.0345) **b) Configuration B (Ro=0.0345)**

c) Configuration C (Ro=0.0345) **d) Configuration D (Ro=0.0099)**

Fig. 6 Nusselt number distribution along the channel centerline ($Re = 19,000$).

edge due to flow reattachment and multiple vortex pairs as discussed above. Generally, TS cases show higher Nusselt distributions than ST or LS cases due to Coriolis and rotational buoyancy forces.

Comparing Fig. 6a (configuration A, $d/D = 0.185$) with Fig. 6b (configuration B, $d/D = 0.333$), the deeper dimple case (configuration B) shows a much higher Nusselt number near the dimple downstream edge and between dimples. That is caused by the enhanced secondary flows ejected from the dimples and the three-dimensional turbulence effect for the deeper dimple cases as discussed by Burgess and Nigrani [10]. The deeper dimple case (configuration B) shows a much higher peak Nusselt number, but, due to the relatively strong flow recirculation, the minimum Nusselt number on the cavity floor near the upstream dimple edge is lower than that for configuration A.

The effect of dimple center-to-center distance on heat transfer can be seen by observing Fig. 6a (configuration A, $S/D = 1.2$) and Fig. 6c (configuration C, $S/D = 1.5$). The Nusselt numbers on the dimple cavity floor and near dimple for both configurations are similar. But compared with configuration A, the effect of rotating directions for configuration C is not significant because of the diminished flow turbulating effect by the sparsely distributed dimples.

Figure 6d shows the Nusselt number distribution along the center line of the channel with smaller channel height (configuration D, $H/D = 0.625$). Compared with configuration A ($H/D = 1.23$), the Nusselt number is higher for configuration D (especially downstream rims of each dimple) and that is caused by the enhancement of vortex pairs which are periodically shed from the dimples for lower channel height as discussed by Mahmood and Ligrani [8].

Another feature shown in Fig. 6d is that the overall Nusselt number is not as sensitive to rotating direction as that for other configurations and that is caused by the relatively weaker rotating effect. Note that the rotation number for the configuration D (Fig. 6d) is less than one third of the rotation number of configuration A. Because of the low rotating number, relatively stronger vortices and mainstream momentum, the effects of rotating on the Nusselt number distribution for configuration D are diminished.

Figure 7 presents the averaged Nusselt number for different dimple configurations and channel heights. For all tested Reynolds numbers, deeper dimples gave higher averaged Nusselt numbers as shown in Fig. 7a due to increased vortex strength and turbulent transport [10]. Because of the increased flow disturbance by densely distributed dimples, the averaged Nusselt numbers for $S/D = 1.2$ cases are higher than those for $S/D = 1.5$ cases (Fig. 7b). The effect of dimple depth and dimple center-to-center distance on heat transfer augmentation is more significant for TS cases as shown in Figs. 7a and 7b. Because the heat transfer augmentation by deeper or densely distributed dimples is proportional to the local air velocity, the heat transfer on the dimpled surface for TS cases could be further increased by increased air velocity, by Coriolis force and by centrifugal buoyancy force.

Figure 7c is the averaged Nusselt numbers for two different channel height cases. For all tested Reynolds number cases, the averaged Nusselt numbers for lower channel cases are higher than

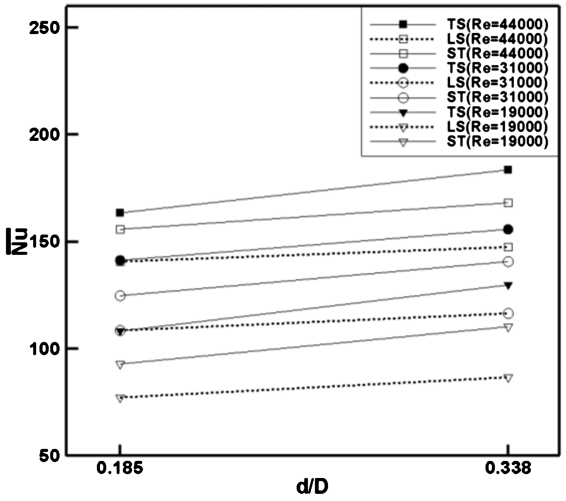

a) Effect of dimple depth

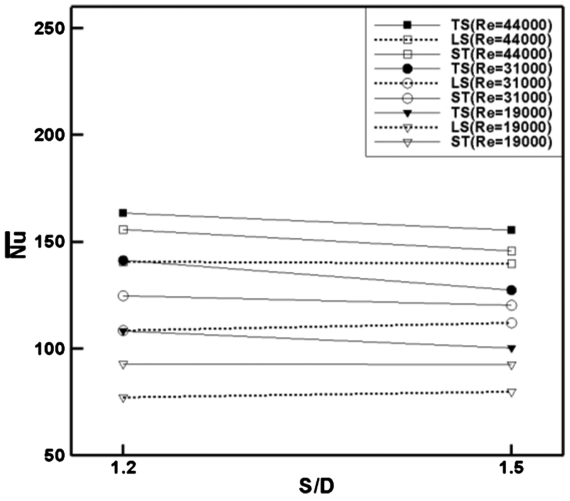

b) Effect of dimple center-to-center distance

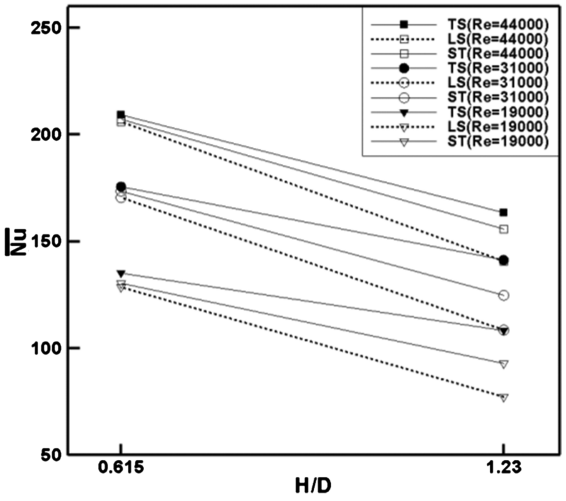

c) Effect of channel height

Fig. 7 Averaged Nusselt numbers for different dimple configurations and channel heights.

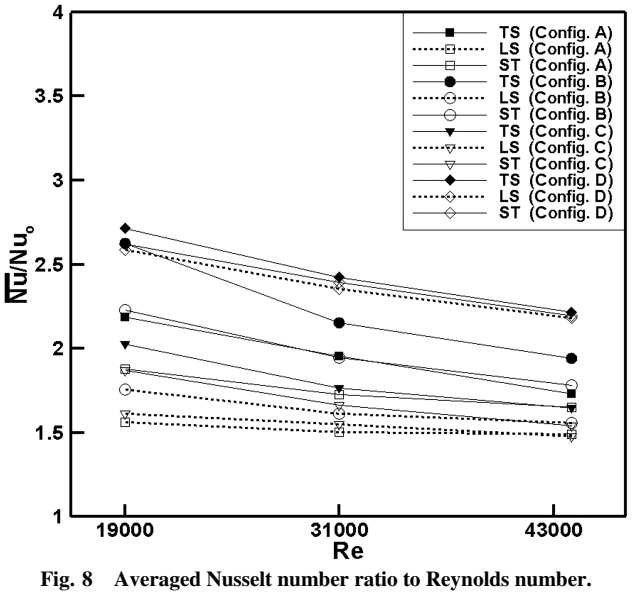

Fig. 8 Averaged Nusselt number ratio to Reynolds number.

those for the higher channel cases. As explained above, increased air velocity and vortex strength due to the lower channel increase heat transfer on the dimpled surface. The effect of channel height is more significant for the LS cases. For LS cases with higher channel height, the flow can relatively easily be pushed away from the leading surface and heat transfer augmentation on the dimpled surface becomes much lower.

Figure 8 shows the averaged Nusselt number ratio calculated by Eqs. (4) and (5). For all tested cases, the Nusselt number ratio is higher than 1.5 and inversely proportional to the Reynolds number. For same dimple configuration or channel height, the Nusselt number ratio is highest for the TS case. For the same Reynolds number case, deeper dimples (configuration B) and narrower channels (configuration D) show the best Nusselt number ratios. The effect of rotating direction is more significant at lower Reynolds numbers because of the relatively higher rotation number (rotating effect).

Figure 9 is the comparison of the averaged Nusselt number ratio of present study and other references. Note that only qualitative comparison is possible because the tested dimple configuration, channel aspect ratio, and test conditions are different. For both present study and Griffith et al. [7], TS case shows higher overall Nusselt number ratio followed by ST and LS case. Results from Mahmood and Ligrani [8] indicate that the averaged Nusselt number ratio is higher for the smaller H/D and same trend can be found by comparing configurations A and D. Also higher averaged Nusselt number ratio is observed for deeper dimple cases (configuration B of

	Present study	d/D	H/D	Rotation
	Configuration A	0.18	1.23	ST
	Configuration B	0.33	1.23	TS, LS,ST
	Configuration D	0.18	0.615	ST
Data No.	Reference	d/D	H/D	Rotation
1	Mahmood and Ligrani [8]	0.2	0.5	ST
2	Mahmood and Ligrani [8]	0.2	1	ST
3	Bergess and Ligrani [10]	0.1	1	ST
4	Bergess and Ligrani [10]	0.2	1	ST
5	Bergess and Ligrani [10]	0.3	1	ST
6	Griffith et al [7]	0.3	2	ST
7	Griffith et al [7]	0.3	2	TS
8	Griffith et al [7]	0.3	2	LS

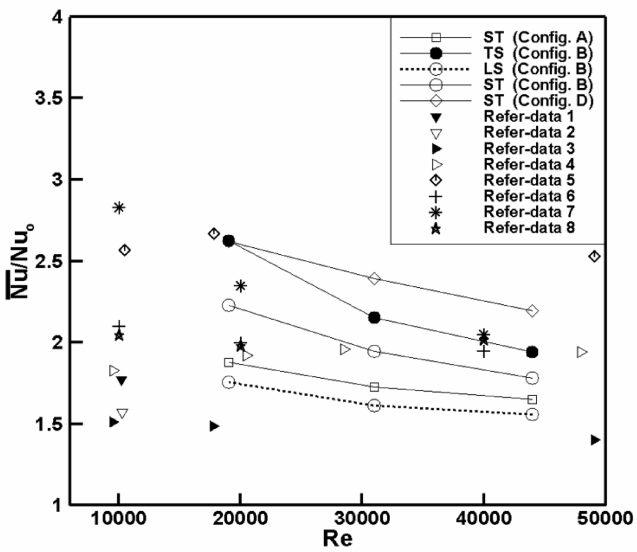

Fig. 9 Comparison of Nusselt number ratio of the present study with other experimental results.

present study and Bergess and Ligrani [10]). Though there are discrepancies between the data of present study and references, both data show similar trends as dimple depth ratio (d/D), channel height ratio (H/D), or rotating condition is changed.

Figure 10 presents friction factor ratio calculated by Eqs. (6) and (7). As indicated in Fig. 2a, pressure taps were located at the dimpled surface, but the measured pressure was not affected by the rotating direction. Compared with configuration A, the friction factor ratio is higher for deeper dimple case (configuration B) and low channel height case (configuration D). As the dimple center-to-center distance is increased (configuration C), the friction factor ratio was decreased. For all cases, the friction factor ratio increases as the Reynolds number increases.

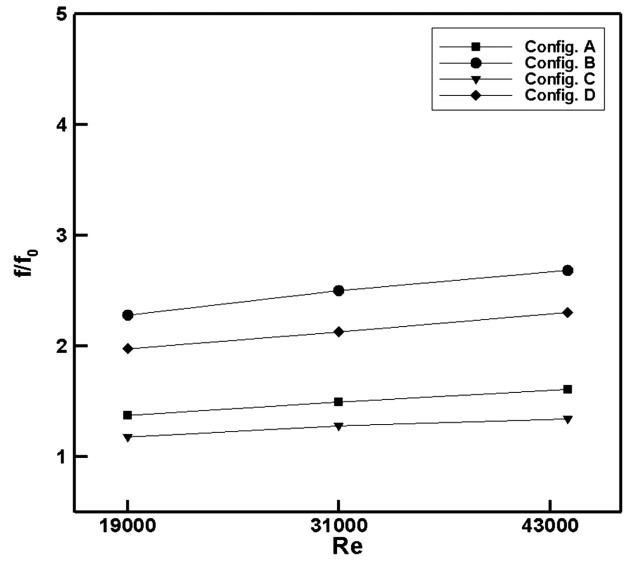

Fig. 10 Friction factor ratio to Reynolds number.

V. Conclusions

The detailed distribution of heat transfer coefficients in a rotational dimpled channel was measured using the transient liquid crystal technique. The channel rotating speed was fixed at 500 rpm and the effects of dimple depth, dimple center-to-center distance, channel height, rotating direction, and Reynolds number on heat transfer augmentation were investigated. The principal conclusions of the current study are summarized as follows:

1) The Nusselt number ratio increased as the Reynolds number decreased for all tested cases and this trend was significant for TS cases due to the higher rotating effect at lower Reynolds number.

2) For the same dimple configuration and channel height, Nusselt numbers for TS cases were the highest because of increased flow velocity near the dimpled surface due to Coriolis and rotational buoyancy forces.

3) Nusselt numbers for deeper dimple cases showed higher values, especially in the TS case.

4) Compared with the sparsely distributed dimple cases, densely distributed dimple cases showed higher Nusselt numbers for all rotating directions and Reynolds numbers.

5) The overall Nusselt number for lower channel cases was higher because of the enhanced vortex pairs.

The results of the current study were obtained at lower rotating speeds and rotation numbers than those for a real gas turbine. Also, due to the limitation of the test technique, the effect of density ratio could not be considered. Cautions should be taken to apply the presented data. However, the detailed distribution of the heat transfer coefficient on a rotating dimpled channel is not easy to find in open literature, and the authors hope that the presented data can be used for validation of CFD results. Research on higher rotation numbers is in progress and will be presented in the near future.

Acknowledgment

This work has been supported by the Korean Electrical Engineering and Science Research Institute, 2008T00100161), which is funded by the Korean government (Ministry of Knowledge Economy).

References

[1] Han, J. C., Dutta, S., and Ekkad, S. V., *Gas Turbine Heat Transfer and Cooling Technology*, Taylor and Francis, New York, 2000.

[2] Han, J. C., "Turbine Blade Cooling Studies at Texas A&M University: 1980-2004," *Journal of Thermophysics and Heat Transfer*, Vol. 20, No. 2, 2006, pp. 161–187. doi:10.2514/1.15403

[3] Belen'kiy, M. YA., Gotovskiy, M. A., Lekakh, B. M., Fokin, B. S., and Dolgushin, K. S., "Heat Transfer Augmentation Using Surfaces Formed by a System of Spherical Cavities," *Heat Transfer Research*, Vol. 25, No. 2, 1993, pp. 196–203.

[4] Moon, H. K., O'Connell, T., and Glezer, B., "Channel Height Effect on Heat Transfer and Friction in a Dimpled Passage," *Journal of Engineering for Gas Turbines and Power*, Vol. 122, No. 2, 2000, pp. 307–313. doi:10.1115/1.483208

[5] Mahmood, G. I., Hill, M. L., Nelson, D. L., Ligrani, P. M., Moon, H.-K., and Glezer, B., "Local Heat Transfer and Flow Structure on and Above a Dimpled Surface in a Channel," *Journal of Turbomachinery*, Vol. 123, No. 1, 2001, pp. 115–123. doi:10.1115/1.1333694

[6] Moon, S. W., and Lau, S. C., "Turbulent Heat Transfer Measurements on a Wall with Concave and Cylindrical Dimples in a Square Channel," ASME Paper GT-2002-30208, 2002.

[7] Griffith, T. S., Al-Hadhrami, L., and Han, J. C., "Heat Transfer in Rotating Rectangular Cooling Channels (AR = 4) with Dimples," *Journal of Turbomachinery*, Vol. 125, No. 3, 2003, pp. 555–563. doi:10.1115/1.1571850

[8] Mahmood, G. I., and Ligrani, P. M., "Heat Transfer in a Dimpled Channel: Combined Influences of Aspect Ratio, Temperature Ratio, Reynolds Number, and Flow Structure," *International Journal of Heat and Mass Transfer*, Vol. 45, No. 10, 2002, pp. 2011–2020. doi:10.1016/S0017-9310(01)00314-3

[9] Wang, Z., Yeo, K. S., and Khoo, B. C., "Numerical Simulation of Laminar Channel Flow over Dimpled Surface," AIAA Paper AIAA 2003-3964, 2003.

[10] Burgess, N. K., and Nigrani, P. M., "Effects of Dimple Depth on Nusselt Numbers and Friction Factors for Internal Cooling in a Channel," ASME Paper GT-2004-54232, 2004.

[11] Khalatov, A., Byerley, A., Ochoa, D., and Min, S. K., "Flow Characteristics within and Downstream of Spherical and Cylindrical Dimple on a Flat Plate at Low Reynolds Numbers," ASME Paper GT2004-53656, 2004.

[12] Ligrani, P. M., Burgess, N. K., and Won, S. Y., "Nusselt Numbers and Flow Structure on and Above a Shallow Dimpled Surface Within a Channel Including Effects of Inlet Turbulence Intensity Level," ASME Paper GT2004-54231, 2004.

[13] Shin, S., Lee, K. S., Park, S. D., and Kwak, J. S., "Measurement of the Heat Transfer Coefficient in the Dimpled Channel: Effects of Dimple Arrangement and Channel Height," *Journal of Mechanical Science and Technology*, Vol. 23, 2009, pp. 624–630.

[14] Slabaugh, C. D., Le, A. P., and Kapat, J. S., "A Study of Side Wall Heat Transfer Augmentation in a Narrow Rectangular Duct," AIAA Paper AIAA 2009-5377, 2009.

[15] Elyyan, M. A., and Tafti, D. K., "Effect of Coriolis Forces in a Rotating Channel with Dimples and Protrusions," *International Journal of Heat and Fluid Flow*, Vol. 31, No. 1, 2010, pp. 1–18. doi:10.1016/j.ijheatfluidflow.2009.10.002

[16] Incropera, F. P., and DeWitt, D. P., "Heat and Mass Transfer," 5th ed., Wiley, New York, 2001.

[17] Wagner, G., Kotulla, M., Ott, P., Weigand, B., and von Wolfersdorf, J., "The Transient Liquid Crystal Technique: Influence of Surface Curvature and Finite Wall Thickness," *Journal of Turbomachinery*, Vol. 127, 2005, pp. 175–182. doi:10.1115/1.1811089

[18] Moffat, R. J., "Describing the Uncertainties in Experimental Results," *Experimental Thermal and Fluid Science*, Vol. 1, No. 1, 1988, pp. 3–17.